RSC Advances

PAPER

View Article Online
View Journal | View Issue

Cite this: *RSC Adv.*, 2017, **7**, 4746

Facile synthesis of amine-functionalized SBA-15-supported bimetallic Au–Pd nanoparticles as an efficient catalyst for hydrogen generation from formic acid†

Lixin Xu,[a] Fang Yao,[a] Jili Luo,[b] Chao Wan,*[a] Mingfu Ye,[a] Ping Cui*[a] and Yue An[c]

Received 14th November 2016
Accepted 27th December 2016

DOI: 10.1039/c6ra26793a

www.rsc.org/advances

In this study, a series of amine-functionalized SBA-15-supported bimetallic Au–Pd nanoparticles (Au–Pd/SBA-15-Amine) as catalysts are successfully synthesized by surface functionalization and co-reduction and characterized by inductively coupled plasma-atomic emission spectroscopy, XRD, XPS, and TEM. The Au–Pd/SBA-15-Amine catalysts thus obtained are tested for the dehydrogenation of formic acid (FA)–sodium formate (SF). Among the tested Au–Pd/SBA-15-Amine catalysts, as-synthesized Au_2Pd_8/SBA-15-Amine exhibits 100% H_2 selectivity and outstanding catalytic activity with an initial turnover frequency (TOF) of 1786 h^{-1} at 323 K; this superior catalytic activity is attributed to synergy between Au–Pd and SBA-15-Amine and the promotion effect of SF. At SF concentrations of greater than 0.5 mol L^{-1}, SF can partially participate in dehydrogenation. The facile synthesis of the Au–Pd/SBA-15-Amine catalyst is imperative for accelerating the widespread application of FA–SF mixtures as a promising hydrogen carrier.

Introduction

In the past decades, the search for sustainable, renewable energies has increased owing to the widespread utilization of conventional fossil fuels, which has resulted in serious environmental and energy problems.[1,2] Hydrogen, which is the most abundant element in nature, has been recognized as a promising and green energy source,[3–5] attributed to its outstanding energy density of as high as 142 MJ kg^{-1}—nearly three times greater than that of fossil fuels (55 MJ kg^{-1}).[6,7] Furthermore, with the use of hydrogen in a fuel cell, water is produced as the only by-product.[8] Despite these advantages, the economical, efficient, and safe production and storage of hydrogen remain challenges for the current development of hydrogen energy.

In recent years, considerable efforts have been focused on the development of novel materials that can store hydrogen and recycling liberation.[9–12] In this regard, several liquid materials, such as hydrous hydrazine,[13–15] formic acid (FA),[16–19] *N*-ethylcarbazole,[20,21] and methanol,[22,23] have attracted considerable attention as hydrogen storage materials; these materials can be easily handled and stored. Particularly, FA has attracted increasing attention, attributed to the fact that as compared with other substrates, it is less hazardous, and it can be recycled by the hydrogenation of carbon dioxide (CO_2).[24–27] In general, the decomposition of FA occurs *via* dehydrogenation (1) and dehydration (2):[28–30]

$$HCOOH\ (l) \rightarrow CO_2\ (g) + H_2\ (g);\ \Delta G_{298\ K} = -48.8\ kJ\ mol^{-1} \quad (1)$$

$$HCOOH\ (l) \rightarrow CO\ (g) + H_2O\ (g);\ \Delta G_{298\ K} = -28.5\ kJ\ mol^{-1} \quad (2)$$

Nevertheless, carbon monoxide (CO), which degrades catalyst performance, can also be generated by reaction (2), which should be strictly controlled. These two routes can be affected by several factors, such as reaction temperature, selected catalysts, as well as the pH of reaction mixture.[31–33] Thus, it is highly desirable to design and fabricate catalysts exhibiting excellent performance for the dehydrogenation of FA.

It has been previously reported that, Pd-based bimetallic nanoparticles (NPs), especially those combined with Au, Ni, Ag, and Co, have been reported to demonstrate exhibit highly efficient catalytic performance for the dehydrogenation of FA.[34–42] Chen *et al.*[43] have reported the reduction of mixed noble-metal precursors under ice-water bath conditions and successfully synthesized Au–Pd alloy nanoparticles, which were well-dispersed on carbon black using the reduction of mixed noble-metal precursors under ice-water bath conditions, these nanoparticles which exhibited a high activity and selectivity with an initial turnover frequency (TOF) as high as 635 h^{-1} at

[a]College of Chemistry and Chemical Engineering, Anhui University of Technology, 59 Hudong Road, Ma'anshan 243002, China. E-mail: wanchao1219@hotmail.com; cokecp@outlook.com; Fax: +86 555 2311822; Tel: +86 555 2311807

[b]PetroChina Huabei Oilfield Company Gas Storage Management Service, 15 Battle Road, Renqiu 062550, China

[c]College of Chemical and Biological Engineering, Zhejiang University, 38 Zheda Road, Hangzhou 310027, China

† Electronic supplementary information (ESI) available. See DOI: 10.1039/c6ra26793a

nearly 273 K. Jiang *et al.*[44] have reported a facile and, green strategy for the synthesis of growing ultrafine Au@Pd core–shell nanoclusters, with exhibiting a good dispersity, grown on nitrogen-doped mildly reduced graphene oxide (Au@Pd/N-mrGO) without an additional reducing agent and any surfactant. This catalyst exhibits 100% hydrogen selectivity and superior catalytic performance for the decomposition of an FA aqueous solution at 298 K without the introduction of any additive at 298 K. Zahmakiran *et al.*[45] have presented the use of a heterogeneous catalyst system consisting of amine-functionalized SiO_2 as the carrier, which supported a physical mixture of a PdAu alloy and MnO_x NPs with an average diameter of 2.2 nm. This PdAu–MnO_x/N-SiO_2 catalyst was used for the decomposition of FA without an additive, in which good performance was achieved with a TOF of up to 860 mol H_2 (mol catalyst)$^{-1}$ h^{-1}. Furthermore, it was concluded that the support has been confirmed to play a decisive role in the dehydrogenation reaction.

The surface functionality of the support, such as the amine groups, served as interaction sites for sustaining metallic nanoclusters and co-catalytic species, which can act as deprotonation sites for FA molecules in the dehydrogenation of FA.[46–49] Jiang *et al.*[50] have prepared a Au–Pd–MnO_x nanocomposite anchored on a bi-support (ZIF-8-rGO) consisting of a zeolitic imidazolate framework (ZIF-8) and reduced graphene oxide by a simple wet-chemical method; this catalyst exhibits good catalytic activity for the generation of hydrogen from high-concentration FA in the absence of additive at 298 K, the TOF was as high as 382.1 mol H_2 (mol catalyst)$^{-1}$ h^{-1} without additives. Asefa *et al.*[51] have revealed a facile route for synthesizing ultrasmall Pd NPs immobilized on amine-functionalized SBA-15 (SBA-15-Amine/Pd), which exhibit high activity for the dehydrogenation of FA with a high TOF of 293 h^{-1} at ambient temperature.

Herein, for the first time, we report the synthesis of Au–Pd NPs dispersed on SBA-15-Amine by the dehydrogenation of FA–SF *via* co-reduction. Au–Pd/SBA-15-Amine exhibits excellent activity and satisfactory stability for the production of hydrogen from FA; it is markedly superior to the other catalysts reported thus far.

Experimental section

Materials

Anhydrous ethanol (C_2H_5OH, AR), potassium chloride (KCl, AR), hydrochloric acid (HCl, AR), sodium formate (SF, HCOONa, AR), formic acid (HCOOH, AR), toluene (C_7H_8, AR), and calcium hydride (CaH_2, AR) were obtained from Sinopharm Chemical Reagent Co., Ltd. SBA-15 were obtained from Nanjing XFNANO Materials Tech Co., Ltd. Chloroauric acid ($HAuCl_4 \cdot 4H_2O$, AR) and palladium chloride ($PdCl_2$, AR) were supplied from Nanjing Chemical Reagent Co., Ltd. Deionized water was obtained by reverse osmosis, followed by ion exchange and filtration. Toluene was distilled over calcium hydride for removing marginal amounts of water and stored in a vacuum glove box under nitrogen. All other reagents were utilized as received without further purification.

Synthesis of SBA-15-Amine

First, 1.0 g of SBA-15 was dispersed into 50 g of anhydrous toluene, followed by the addition of 13.7 mmol of 3-aminopropyltriethoxysilane (APTES) under stirring. Second, the resulting slurry was refluxed for 24 h at 353 K for grafting the mesoporous channel surfaces of SBA-15 with primary amine groups. Next, after filtration, the solid product was repeatedly washed with toluene and ethanol and allowed to dry at 298 K. Finally, APTES-grafted SBA-15 was obtained, hereafter referred to as SBA-15-Amine.[52]

Synthesis of AuPd/SBA-15-Amine

Bimetallic Au–Pd/SBA-15-Amine was prepared as follows. First, 1 g $PdCl_2$ was added to 100 mL KCl (0.84 g, 2 equiv. with respect to $PdCl_2$) at 298 K and completely dissolved to form potassium tetrachloropalladinic acid (60 mM, K_2PdCl_4) solution under stirring. Second, 1 g SBA-15-Amine was added to the metal precursor solution containing both $HAuCl_4$ (0.24 mmol) and the K_2PdCl_4 (0.16 mmol) solution and stirred for 24 h for impregnating the metal on SBA-15-Amine at 298 K. The resulting slurry was reduced with sodium borohydride ($NaBH_4$) and stirred at 273 K for 4 h. Finally, the mixture was filtered and washed several times, followed by drying the resulting solid at 373 K. Hereafter, the solid catalyst thus obtained was denoted as Au_6Pd_4/SBA-15-Amine. For comparison, the amounts of $HAuCl_4$ and K_2PdCl_4 were varied with the desired Au–Pd atomic ratio, and the nominal total metal loading was 0.4 mmol. Au/SBA-15-Amine, Pd/SBA-15-Amine, Au_8Pd_2/SBA-15-Amine, Au_6Pd_4/SBA-15-Amine, Au_4Pd_6/SBA-15-Amine, and Au_2Pd_8/SBA-15-Amine were prepared in a similar manner.

Hydrogen generation from FA/SF over AuPd/SBA-15-Amine

The production of hydrogen from an FA–SF solution was conducted in a glass tube at a preset temperature (303–333 K) under ambient atmosphere. Typically, 100 mg of a catalyst was placed into a stirred glass tube, followed by the rapid injection of 2 mL of an FA–SF mixture solution containing FA (3 mmol) and SF (1 mmol). A gas burette filled with water was connected to the reaction vessel for measuring the volume of released gas. The dehydrogenation performance of FA–SF over all catalysts was conducted following the same procedure.

CO_2 trap

For confirming the molar ratios of H_2 and CO_2 in the gas mixture obtained *via* the dehydrogenation of an aqueous FA–SF solution over Au–Pd/SBA-15-Amine, the gas generated during the reaction was passed through a NaOH trap (10 M NaOH solution), and its volume was monitored using a gas burette.

Stability test

For the recycling stability test, 2 mL of FA–SF was added into a stirred glass tube after completing the first run of the dehydrogenation of FA–SF; these stability tests were repeatedly conducted by the addition of fresh FA (3 mmol) to the reaction flask.

Calculation of turnover frequency (TOF)

The initial TOF reported here is calculated by the total amount of gas volume (H_2 + CO_2) when x_a reaches 20% from the following equation:[41]

$$x_a = \frac{P_{atm} V}{2RTn_{FA}}$$

$$TOF = \frac{P_{atm} V}{2RTn_{Ag+Pd}\, t}$$

here, P_{atm} is the atmospheric pressure (101 325 Pa), V is the generated volume of (H_2 + CO_2) gas, R is the universal gas constant (8.3145 m^3 Pa mol^{-1} K^{-1}), T is the room temperature (298 K), n_{Ag+Pd} is the total mole number of Ag and Pd atoms in the catalyst, and t is the initial time of the catalytic reaction when x_a reaches 20%.

Characterization

The chemical composition of the catalysts was investigated using a Thermo iCAP6300 inductively coupled plasma-atomic emission spectroscopy (ICP-AES). Powder X-ray diffraction (XRD) patterns were recorded on a Bruker D8-Advance XRD instrument using a Cu Kα radiation source (λ = 0.154178 nm) with a velocity of 1° min^{-1}. XPS measurements were conducted on a Thermo Scientific Escalab 250Xi spectrometer equipped with an Al Kα radiation source (1486.6 eV, 15 kV). All binding energies were calibrated with the C 1s peak at 284.8 eV for adventitious carbon. TEM images were obtained using an FEI Tecnai F20 TEM with a working voltage of 200 kV. Detailed gas for released from dehydrogenation were analyzed using a GC-9860 II (Shanghai Qiyang Information Technology Co., Ltd.) with a TCD for CO_2 and H_2 and a flame ionization detector (FID)–methanator for CO (detection limit: ~10 ppm for CO).

Results and discussion

As the pore walls of SBA-15 are covered with residual surface silanols (≡Si–OH), SBA-15 can be functionalized with organic functional groups, which are beneficial for anchoring metal ions to the SBA-15 surfaces.[52] Hence, these surfaces are modified using APTES; this APTES-functionalized SBA-15 is referred to as SBA-15-Amine.[52] As shown in the scheme in Fig. 1, a series of Au–Pd/SBA-15-Amine catalysts are synthesized by a surfactant-free co-reduction method. Specifically, SBA-15-Amine is first added to a precursor solution containing $HAuCl_4$ and K_2PdCl_4 and stirred to impregnate Au^{3+} and Pd^{2+} into the SBA-15-Amine surface. Second, $NaBH_4$ is added for reducing the metal precursor under ice-water bath conditions. Next, the resultant solution is centrifuged and washed with copious

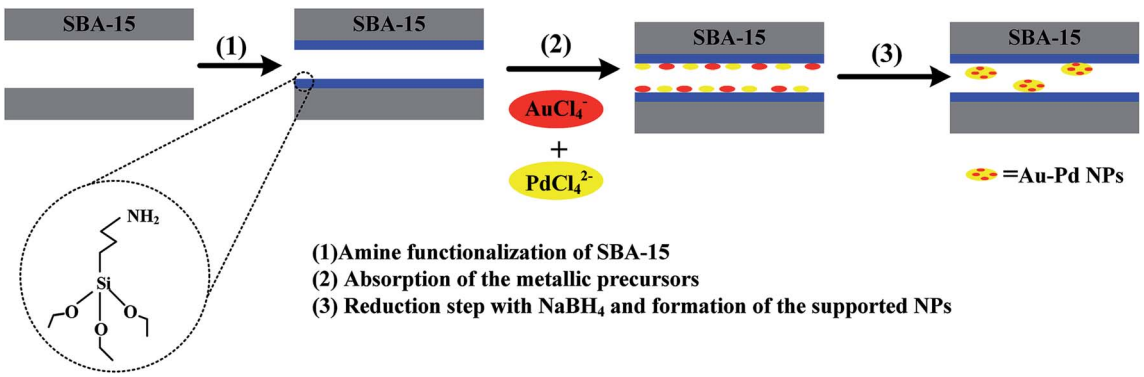

Fig. 1 Schematic illustration for the synthesis of the supported Au–Pd/SBA-15-Amine.

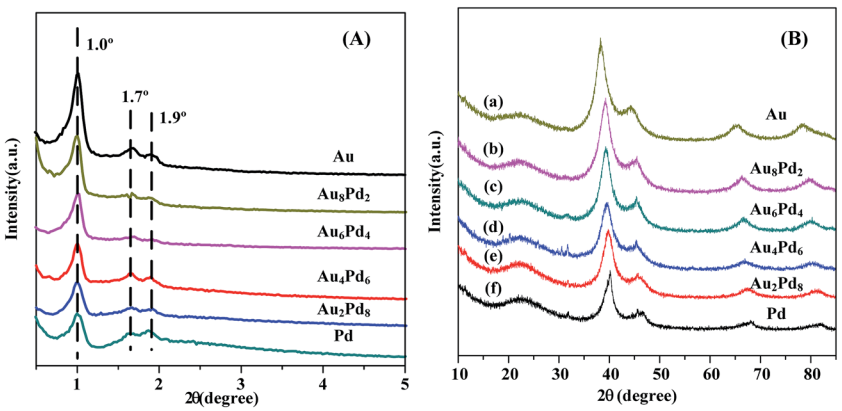

Fig. 2 (A) Small-angle and (B) wide-angle XRD pattern of all as-prepared catalysts supported SBA-15-Amine with different molar ratio of Au/Pd.

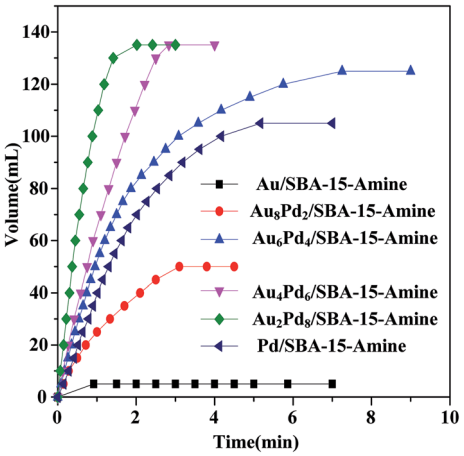

Fig. 3 Time course plots for hydrogen generation from FA/SF over Au–Pd/SBA-15-Amine with different molar ratio of AuPd (n_{FA} = 3 mmol, n_{SF} = 1 mmol).

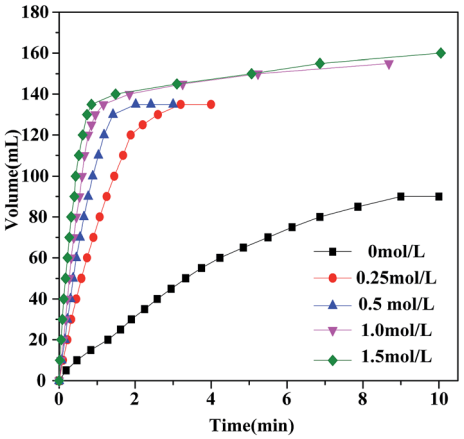

Fig. 4 Hydrogen generation by decomposition of FA/SF with different SF concentration catalyzed by Au_2Pd_8/SBA-15-Amine at 323 K (n_{FA} = 3 mmol).

amounts of water. Finally, the solid thus obtained is dried in a vacuum oven at 373 K for 10 h. The compositions of catalysts are modified by controlling the molar ratio of Au^{3+}–Pd^{2+} in the precursor solution, as confirmed by ICP-AES. Table S1† summarizes the ICP-AES results obtained for catalyst compositions.

Fig. 2 shows the small- and wide-angle XRD patterns of Au/SBA-15-Amine, Au_8Pd_2/SBA-15-Amine, Au_6Pd_4/SBA-15-Amine, Au_4Pd_6/SBA-15-Amine, Au_2Pd_8/SBA-15-Amine, and Pd/SBA-15-Amine. As shown in Fig. 2(A), three well-resolved diffraction peaks are observed for all catalysts: a very strong peak at 2θ = 1.02° and two weak peaks at 2θ = 1.68° and 2θ = 1.95°, attributed to the (100), (110), and (200) planes, respectively; these three peaks indicate that there is no evidence of any alteration in the ordered two-dimensional hexagonal structure of Au–Pd/SBA-15-Amine during catalyst synthesis.[52,53] As can be observed from Fig. 2(B), a broad diffraction peak at 2θ = 22.3° is observed for all catalyst samples, which corresponds to the presence of silica and can be assigned to the amorphous SBA-15 framework.[52,53] Furthermore, diffraction peaks for Au–Pd/SBA-15-Amine are observed between those for bulk Au and Pd supported on SBA-15-Amine (JCPDS, 65-8601 and 65-2867), suggesting the formation of Au–Pd alloy structure.[45,50,54,55]

Fig. 3 and Table S2† show the performance of Au–Pd/SBA-15-Amine at different molar ratios of Au–Pd for the dehydrogenation of an FA–SF solution at 323 K. As shown, catalytic activity is predominantly affected by the molar ratios of Au–Pd in Au–Pd/SBA-15-Amine. Particularly, Au_2Pd_8/SBA-15-Amine exhibits the best activity of all of the tested catalysts, where FA produces the theoretical gas volume within only 2 min at 323 K. The corresponding TOF is as high as 1786 h^{-1}, which is significantly greater than most of the TOFs reported previously for other Au–Pd catalysts used for the decomposition of FA (Table S3†). Alloy formation between Au and Pd exerts a positive synergistic effect on dehydrogenation, which is consistent with that reported in previous studies.[45,50,54,56] Moreover, as shown in Fig. S1–S3,† the composition of the produced gas is identified by GC analysis and a 10 NaOH solution trap. As shown in Fig. S1,† the gas volume is reduced to half after treatment with the NaOH trap,

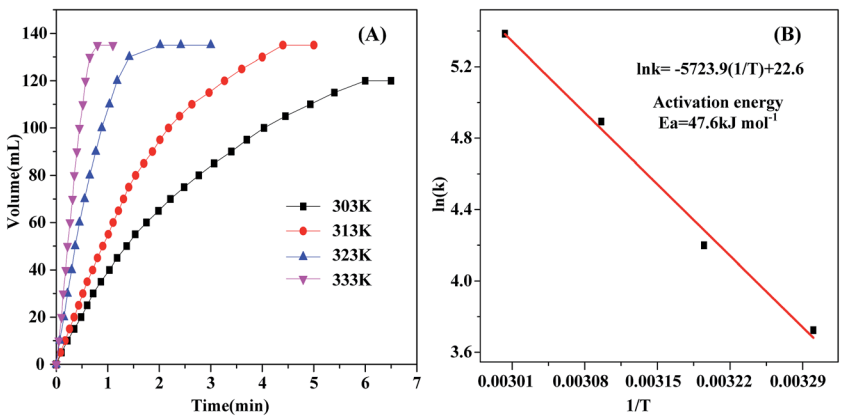

Fig. 5 (A) Time course plots for hydrogen release by the dehydrogenation of FA/SF by Au_2Pd_8/SBA-15-Amine at 303 K, 313 K, 323 K and 333 K. (B) Plot of ln *k* *vs.* 1/*T* for Au_2Pd_8/SBA-15-Amine (n_{FA} = 3 mmol, n_{SF} = 1 mmol).

confirming that dehydrogenation results in the generation of hydrogen and carbon dioxide, not CO, which is in agreement with GC analysis shown in Fig. S2 and S3.†

The SF concentration plays an important role in the enhancement of catalytic performance for the dehydrogenation of FA, as has been reported in previous studies.[45,49] From Fig. 4, using Au_2Pd_8/SBA-15-Amine without SF, only 66.7% of SF is decomposed into hydrogen in 9 min with a TOF of 207 h^{-1}. On the other hand, the catalytic performance for Au_2Pd_8/SBA-15-Amine is significantly improved by the introduction of SF into the reaction system. With increasing SF concentration from 0 to 0.5 mol L^{-1} (FA–SF molar ratio = 3 : 1), FA from the FA–SF solution completely reacts, resulting in the production of a theoretical gas volume of 135 mL, while SF is not involved in dehydrogenation. Moreover, at SF concentrations of greater than 0.5 mol L^{-1}, SF partially participates in dehydrogenation. The dehydrogenation rate and efficiency of FA are concluded to be enhanced with increasing SF concentration, and SF is involved in the decomposition reaction at a high SF concentration (>0.5 mol L^{-1}).

The decomposition of FA–SF catalyzed by Au_2Pd_8/SBA-15-Amine is conducted at various temperatures ranging from 303 K to 333 K; an activation energy (E_a) of 47.6 kJ mol^{-1} is observed, as shown in Fig. 5, which is in agreement with those reported previously.[44,45,50,57,58] In addition, the reusability of the Au_2Pd_8/SBA-15-Amine catalyst is investigated at 323 K. As can be observed in Fig. 6, the catalyst exhibits excellent catalytic performance without a distinct decrease for dehydrogenation activity after five runs.

The surface states of supported Au–Pd NPs are recorded by XPS, and Fig. 7 shows the Au 4f and Pd 3d core level spectra for Au/SBA-15-Amine, Pd/SBA-15-Amine, and Au_2Pd_8/SBA-15-Amine. In the Au 4f spectrum (Fig. 7(A)), two strong peaks are observed at 83.9 and 87.6 eV for Au/SBA-15-Amine, attributed to metallic Au^0. The Au 4f spectrum for Au_2Pd_8/SBA-15-Amine is divided into two peaks—83.5 and 87.1 eV. As compared with that of Au/SBA-15-Amine, the binding energy for Au 4f is shifted to a lower value. From Fig. 7(B), two peaks are observed at 335.8 and 340.8 eV for Pd/SBA-15-Amine, attributed to $3d_{5/2}$ and $3d_{3/2}$ of Pd^0, respectively. The results obtained from the XPS signals of Pd 3d for Au_2Pd_8/SBA-15-Amine exhibit a $3d_{5/2}$ peak at 336.1 eV and a $3d_{3/2}$ peak at 341.5 eV, corresponding to a binding energy greater than that obtained for the Pd 3d of Pd/SBA-15-Amine.[55–57] Thus, these changes in binding energy are attributed to the occurrence of alloying in the supported Au–Pd NPs,[44,45,50,56–58] which are in good agreement with XRD characterization.

Fig. 8(a)–(d) show the typical TEM images of the as-synthesized Au_2Pd_8/SBA-15-Amine catalysts. NPs are well dispersed with an

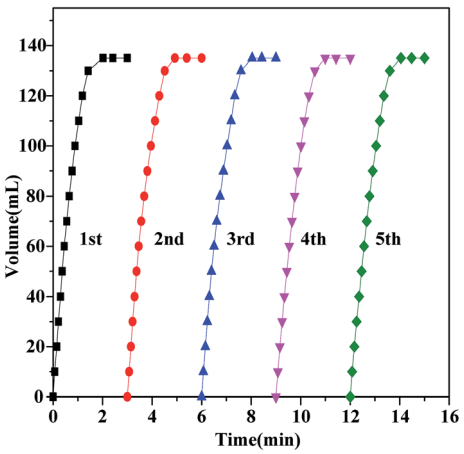

Fig. 6 Reusability test for the hydrogen generation from aqueous FA/SF at 323 K in the presence of Au_2Pd_8/SBA-15-Amine catalyst (n_{FA} = 3 mmol, n_{SF} = 1 mmol).

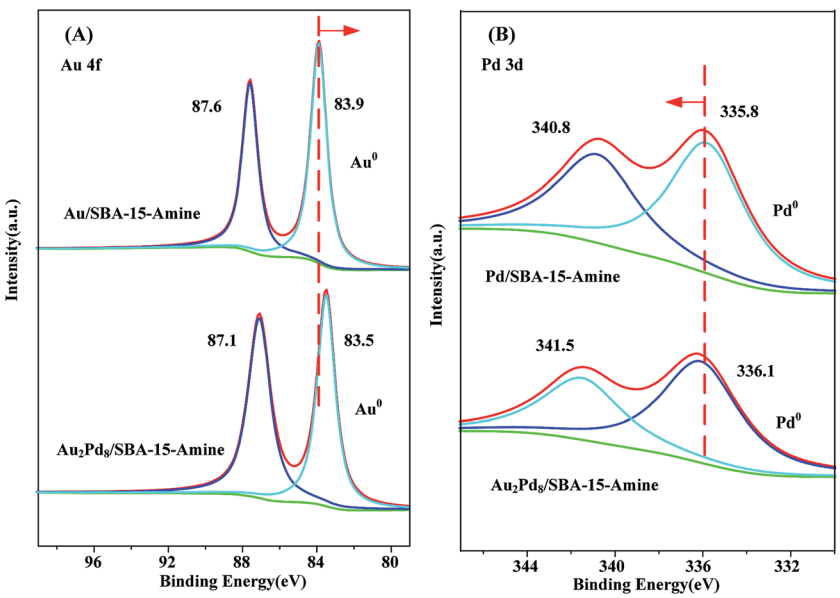

Fig. 7 XPS spectra of (A) Au 4f of Au/SBA-15-Amine and Au_2Pd_8/SBA-15-Amine and (B) Pd 3d of Pd/SBA-15-Amine and Au_2Pd_8/SBA-15-Amine.

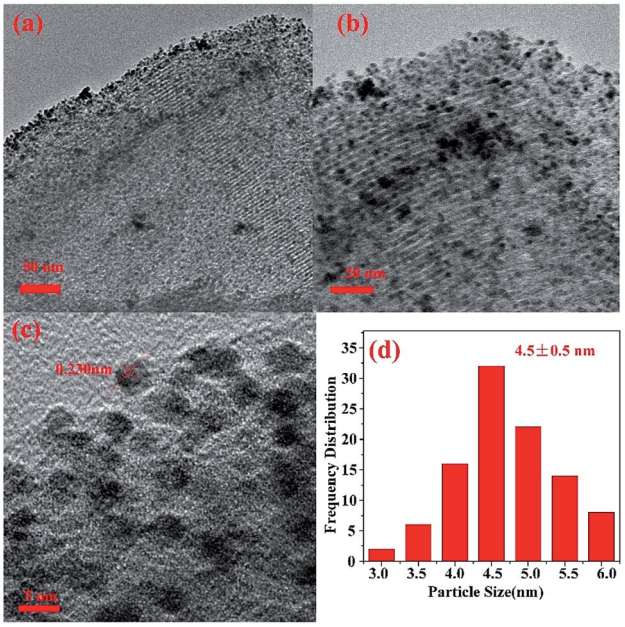

Fig. 8 (a–c) TEM images of Au_2Pd_8/SBA-15-Amine with different magnifications, (d) Au_2Pd_8 nanoparticle size distribution of Au_2Pd_8/SBA-15-Amine, mean size = 4.5 ± 0.5 nm.

average particle size of 4.5 ± 0.5 nm. As shown in the HRTEM image in Fig. 8(c), a lattice spacing of 0.230 nm is observed; this value is between those of the (111) planes of fcc Pd (0.224 nm) and fcc Au (0.235 nm), further suggesting that a Au–Pd NP alloy structure is obtained;[44,45,50,56–58] this result possibly explains the outstanding performance of the prepared catalyst for the dehydrogenation of FA–SF. Results obtained from TEM are consistent with those obtained from XRD and XPS.

Conclusions

In summary, Au–Pd NPs immobilized on SBA-15-Amine were successfully synthesized by surface functionalization and co-reduction. The performance of the as-prepared Au–Pd/SBA-15-Amine catalysts for the dehydrogenation of FA–SF was investigated. The as-synthesized Au_2Pd_8/SBA-15-Amine exhibited 100% H_2 selectivity and superior catalytic performance with an initial TOF of 1786 h^{-1} at 323 K. Furthermore, excellent reusability was achieved. To the best of our knowledge, this outstanding catalytic performance is possibly attributed to the synergistic effect of the Au–Pd alloy in SBA-15-Amine for the catalytic decomposition of FA; this significant enhancement in catalytic performance possibly prompts the large-scale application of FA–SF mixtures as a promising hydrogen-storage material.

Acknowledgements

This work was financially supported by the National Natural Science Foundation of China (21376005, 21476001), Research Fund for Young Teachers of Anhui University of Technology (QZ201610), Anhui Provincial Natural Science Foundation (1608085QF156) and the Scientific Research Foundation of Graduate School of Anhui University of Technology (2016012, 2016017).

References

1 J. A. Turner, *Science*, 2004, **305**, 972–974.
2 W. J. Gan, P. J. Dyson and G. Laurenczy, *ChemCatChem*, 2013, **5**, 3124–3130.
3 P. P. Zhao, N. Cao, J. Su, W. Luo and G. Z. Cheng, *ACS Sustainable Chem. Eng.*, 2015, **3**, 1086–1093.
4 K. Tedsree, T. Li, S. Jones, C. W. A. Chan, K. M. K. Yu, P. A. J. Bagot, E. A. Marquis, G. D. W. Smith and S. C. E. Tsang, *Nat. Nanotechnol.*, 2011, **6**, 302–307.
5 J. M. Petersen, F. U. Zielinski, T. Pape, R. Seifert, C. Moraru, R. Amann, S. Hourdez, P. R. Girguis, S. D. Wankel, V. Barbe, E. Pelletier, D. Fink, C. Borowski, W. Bach and N. Dubilier, *Nature*, 2011, **476**, 176–180.
6 L. Schlapbach and A. Züttel, Hydrogen-storage materials for mobile applications, *Nature*, 2001, **414**, 353–358.
7 D. Bhattacharjee, K. Mandal and S. Dasgupta, *J. Power Sources*, 2015, **287**, 96–99.
8 N. Yi, H. Saltsburg and M. Flytzani-Stephanopoulos, *ChemSusChem*, 2013, **6**, 816–819.
9 Z. J. Zhang, Z. H. Lu and X. S. Chen, *ACS Sustainable Chem. Eng.*, 2015, **3**, 1255–1261.
10 Q. Y. Bi, J. D. Lin, Y. M. Liu, H. Y. He, F. Q. Huang and Y. Cao, *J. Power Sources*, 2016, **328**, 463–471.
11 Q. L. Zhu and Q. Xu, *Energy Environ. Sci.*, 2015, **8**, 478–512.
12 A. Züttel, *Mater. Today*, 2003, **6**, 24–33.
13 L. He, Y. Q. Huang, A. Q. Wang, X. D. Wang, X. W. Chen, J. J. Delgado and T. Zhang, *Angew. Chem., Int. Ed.*, 2012, **51**, 6191–6194.
14 J. Wang, W. Li, Y. R. Wen, L. Gu and Y. Zhang, *Adv. Energy Mater.*, 2015, 1401879.
15 L. X. Xu, N. Liu, B. Hong, P. Cui, D. G. Cheng, F. Q. Chen, Y. An and C. Wan, *RSC Adv.*, 2016, **6**, 31687–31691.
16 M. Hattori, D. Shimamoto, H. Agoa and M. Tsuji, *J. Mater. Chem. A*, 2015, **3**, 10666–10670.
17 C. Fink, M. Montandon-Clerc and G. Laurenczy, *Chimia*, 2015, **69**, 746–752.
18 J. J. A. Celaje, Z. Y. Lu, E. A. Kedzie, N. J. Terrile, J. N. Lo and T. J. Williams, *Nat. Commun.*, 2016, **7**, 11308.
19 J. H. Lee, J. Ryu, J. Y. Kim, S. W. Nam, J. H. Han, T. H. Lim, S. Gautam, K. H. Chae and C. W. Yoon, *J. Mater. Chem. A*, 2014, **2**, 9490–9495.
20 W. Peters, M. Eypasch, T. Frank, J. Schwerdtfeger, C. Körner, A. Bösmann and P. Wasserscheid, *Energy Environ. Sci.*, 2015, **8**, 641–649.
21 C. Wan, Y. An, G. H. Xu and W. J. Kong, *Int. J. Hydrogen Energy*, 2012, **37**, 13092–13096.
22 Q. Liu, L. P. Wu, S. Gülak, N. Rockstroh, R. Jackstell and M. Beller, *Angew. Chem., Int. Ed.*, 2014, **53**, 7085–7088.
23 J. Campos, L. S. Sharninghausen, M. G. Manas and R. H. Crabtree, *Inorg. Chem.*, 2015, **54**, 5079–5084.
24 D. Mellmann, P. Sponholz, H. Junge and M. Beller, *Chem. Soc. Rev.*, 2016, **45**, 3954–3988.

25 A. K. Singh, S. Singh and A. Kumar, *Catal.: Sci. Technol.*, 2016, **6**, 12–40.
26 Ö. Metin, X. L. Sun and S. H. Sun, *Nanoscale*, 2013, **5**, 910–912.
27 T. H. Oh, *Energy*, 2016, **112**, 679–685.
28 Q. L. Zhu, N. Tsumori and Q. Xu, *Chem. Sci.*, 2014, **5**, 195–199.
29 Z. L. Wang, J. M. Yan, H. L. Wang, Y. Ping and Q. Jiang, *Sci. Rep.*, 2012, **2**, 598.
30 K. Mori, M. Dojo and H. Yamashita, *ACS Catal.*, 2013, **3**, 1114–1119.
31 F. Ke, L. H. Wang and J. F. Zhu, *Nanoscale*, 2015, **7**, 8321–8325.
32 Z. L. Wang, J. M. Yan, Y. Ping, H. L. Wang, W. T. Zheng and Q. Jiang, *Angew. Chem., Int. Ed.*, 2013, **52**, 4406–4409.
33 H. M. Dai, N. Cao, L. Yang, J. Su, W. Luo and G. Z. Cheng, *J. Mater. Chem. A*, 2014, **2**, 11060–11064.
34 M. Ojeda and E. Iglesia, *Angew. Chem., Int. Ed.*, 2009, **48**, 4800–4803.
35 Y. Q. Jiang, X. L. Fan, X. Z. Xiao, T. Qin, L. T. Zhang, F. L. Jiang, M. Li, S. Q. Li, H. W. Ge and L. X. Chen, *J. Mater. Chem. A*, 2016, **4**, 657–666.
36 W. Y. Yu, G. M. Mullen, D. W. Flaherty and C. B. Mullins, *J. Am. Chem. Soc.*, 2014, **136**, 11070–11078.
37 Y. L. Qin, J. Wang, F. Z. Meng, L. M. Wang and X. B. Zhang, *Chem. Commun.*, 2013, **49**, 10028–10030.
38 K. Mori, H. Tanaka, M. Dojo, K. Yoshizawa and H. Yamashita, *Chem.–Eur. J.*, 2015, **21**, 12085–12092.
39 Z. L. Wang, H. L. Wang, J. M. Yan, Y. Ping, O. Song-II, S. J. Li and Q. Jiang, *Chem. Commun.*, 2014, **50**, 2732–2734.
40 X. C. Yang, P. Pachfule, Y. Chen, N. Tsumori and Q. Xu, *Chem. Commun.*, 2016, **52**, 4171–4174.
41 M. Yurderi, A. Bulut, N. Caner, M. Celebi, M. Kaya and M. Zahmakiran, *Chem. Commun.*, 2015, **51**, 11417–11420.
42 Z. L. Wang, Y. Ping, J. M. Yan, H. L. Wang and Q. Jiang, *Int. J. Hydrogen Energy*, 2014, **39**, 4850–4856.
43 S. Wu, F. Yang, P. C. Sun and T. H. Chen, *RSC Adv.*, 2014, **4**, 44500–44503.
44 Z. L. Wang, J. M. Yan, H. L. Wang, Y. Ping and Q. Jiang, *J. Mater. Chem. A*, 2013, **1**, 12721–12725.
45 Y. Karatas, A. Bulut, M. Yurderi, I. E. Ertas, O. Alal, M. Gulcan, M. Celebi, H. Kivrak, M. Kaya and M. Zahmakiran, *Appl. Catal., B*, 2016, **180**, 586–595.
46 Q. G. Liu, X. F. Yang, Y. Q. Huang, S. T. Xu, X. Su, X. L. Pan, J. M. Xu, A. Q. Wang, C. H. Liang, X. K. Wang and T. Zhang, *Energy Environ. Sci.*, 2015, **8**, 3204–3207.
47 M. Martis, K. Mori, K. Fujiwara, W. S. Ahn and H. Yamashita, *J. Phys. Chem. C*, 2013, **17**, 22805–22810.
48 S. T. Gao, W. H. Liu, C. Feng, N. Z. Shang and C. Wang, *Catal.: Sci. Technol.*, 2016, **6**, 869–874.
49 A. Bulut, M. Yurderi, Y. Karatas, M. Zahmakiran, H. Kivrak, M. Gulcan and M. Kaya, *Appl. Catal., B*, 2015, **164**, 324–333.
50 J. M. Yan, Z. L. Wang, L. Gu, S. J. Li, H. L. Wang, W. T. Zheng and Q. Jiang, *Adv. Energy Mater.*, 2015, **5**, 1500107.
51 K. Koh, J. E. Seo, J. H. Lee, A. Goswami, C. W. Yoon and T. Asefa, *J. Mater. Chem. A*, 2014, **2**, 20444–20449.
52 A. B. Redondo, M. Ranocchiari and J. A. van Bokhoven, *Dalton Trans.*, 2016, **45**, 2983–2988.
53 Q. L. Yao, Z. H. Lu, K. K. Yang, X. S. Chen and M. H. Zhu, *Sci. Rep.*, 2015, **5**, 15186.
54 C. H. Liu, X. L. Cai, J. S. Wang, J. Liu, A. Riese, Z. D. Chen, X. L. Sun and S. D. Wang, One-step synthesis of AuPd alloy nanoparticles on graphene as a stable catalyst for ethanol electro-oxidation, *Int. J. Hydrogen Energy*, 2016, **41**, 13476–13484.
55 J. J. Feng, L. X. Chen, P. Song, X. L. Wu, A. J. Wang and J. H. Yuan, *Int. J. Hydrogen Energy*, 2016, **41**, 8839–8846.
56 A. K. Singh and Q. Xu, *ChemCatChem*, 2013, **5**, 652–667.
57 S. J. Li, Y. Ping, J. M. Yan, H. L. Wang, M. Wu and Q. Jiang, *J. Mater. Chem. A*, 2015, **3**, 14535–14538.
58 S. Wu, F. Yang, H. Wang, R. Chen, P. C. Sun and T. H. Chen, *Chem. Commun.*, 2015, **51**, 10887–10890.